JTTEE5 23:1323–1332
DOI: 10.1007/s11666-014-0139-5
1059-9630/$19.00 © ASM International

Peer Reviewed

Screening Design of Supersonic Air Fuel Processing for Hard Metal Coatings

C. Lyphout, S. Björklund, M. Karlsson, M. Runte, G. Reisel, and P. Boccaccio

(Submitted March 17, 2014; in revised form July 18, 2014)

Replacement of electrolytic hard chromium method by thermal spray technology has shown a growing interest in the past decades, mainly pioneered by depositing WC-based material by conventional HVOF processes. Lower thermal energy and higher kinetic energy of sprayed particles achieved by newly developed Supersonic Air Fuel system, so-called HVAF-M3, significantly reduces decarburization, and increases wear and corrosion resistance properties, making HVAF-sprayed coatings attractive both economically and environmentally. In the present work, full factorial designs of experiments have been extensively utilized to establish relationships between hardware configurations, process and engineering variables, and coatings properties. The relevance of those process factors is emphasized and their significance is discussed in the optimization of coatings for improved abrasion wear and corrosion performances.

Keywords abrasion wear resistance, corrosion resistance, design of experiments, hard metals, HVAF, WC-based cermets

1. Introduction

In the field of wear, erosion, and corrosion applications, recent restrictions in the use of carcinogenic hexavalent form of chrome element have driven the need of replacing electrolytic hard chrome plating (EHC) by other material/process with equivalent tribological properties (Ref 1). WC- and Cr-based powder materials have been proposed as excellent candidates when processed with high kinetic spraying systems (Ref 2-4). One of the latest low-temperature high-kinetic thermal spray processes, namely Supersonic Air Fuel or HVAF-M3 system (UniqueCoat Technology), emerges as an interesting and promising alternative method to EHC and even to its predecessor HVOF systems (Ref 2-6). The use of compressed air instead of pure oxygen and the fact that grit blasting procedure can be operated with the HVAF-M3 gun itself offers economic advantages well perceived by the industry. Grit blasting by the HVAF-M3 system has therefore been investigated, with particular interest in the improved coating adhesion strength (Ref 6). Recent work on spraying different WC-based powders feedstock with the HVAF-M3 system also revealed coatings with improved tribological properties for wear and corrosion protection in the field of construction equipment and off-shore industries (Ref 2, 7-9). However, apart from the preliminary development of spray conditions specific to a given powder chemistry, no extensive optimization studies of the HVAF-M3 system itself have so far been conducted. Compared to conventional HVOF systems based on tuneable combustion gas parameters settings for a fixed hardware design (Ref 4-6), the HVAF-M3 system is mostly a hardware configuration-based alteration of the process parameters, including (i) hardware configuration (HC) such as the size of the combustion chamber, secondary nozzles, and powder injectors and (ii) process variables (PV) such as fuel pressures, stand-off distance, and powder feed rate. In the present work, process maps have been designed, in order to study factor/response relationships and to highlight the repeatability and reliability of the HVAF-M3 system.

C. Lyphout and **S. Björklund**, University West, Production Technology West, Trollhättan, Sweden; **M. Karlsson**, **M. Runte**, and **G. Reisel**, Oerlikon Metco WOKA GmbH, Barchfeld-Immelborn, Germany; and **P. Boccaccio**, University of Modena and Reggio Emilia, Modena, Italy. Contact e-mail: Christophe.lyphout@hv.se.

2. Experimental Procedure

2.1 Feedstock Materials and Spray Process

A spheroidal, agglomerated and sintered commercial WC-CoCr powder feedstock material WOKA 3654FC (Sulzer Metco), with primary carbides' size of 0.8 μm, was selected for this study. Domex355 substrate coupons, 6 mm thick, were positioned on a rotating carousel, and coated by 10 sequential spray passes. Standard configuration of the HVAF-M3 system was utilized for grit blasting the substrates, i.e., operating the large combustion chamber, long nozzle and short axial powder injector, utilizing mesh 220 (−75 + 45) DURALUM White F220 (Washington Mills). Several combinations of HAVF-M3 HC introduced in the next section were investigated in this study to spray hard metal feedstock powder utilizing Propane as a combustion gas.

2.2 Statistical Models

In this work, design of experiments (DoEs) was used to establish relationships between HVAF-M3 HCs, PV, and coating properties. DoE is a standard statistical approach conventionally used to study relationships between process parameters and coating properties in thermal spray. The approach is usually a stepwise procedure starting with screening fractional or full factorial designs to response surface designs for optimization purposes. In this study, a full factorial design was selected since this design can gain valuable insight in how different process parameters interact on several responses such as deposition temperature and coating microstructure and tribological properties. It should be noted that quantification or discretization of all factors and responses is necessary when using DoE and that the results are dependent on the selected levels of the factors (Table 1). The investigation was performed utilizing the statistical software MODDE ©, MKS Umetrics AB, Sweden. Three full factorial screening designs, comprising 29 experimental runs in total, were performed in a random order to increase the model reliability, reproducibility, and repeatability, including three center points for each design, also called *r*eplicates. Multiple linear regression (MLR) was used to establish the relationships between the factors and the responses. Separate MLR models were derived for each response variable to establish a best fit for the statistical representation of the significance of each factor and their eventual interactions. Three full factorial designs of experiments (DoEs) were selected, all connected by common center points (Table 1). In the first DoE referred as WP1, combustion chamber size, injector length, and nozzle designs were selected as main factors. In the second WP2 DoE, the two injection locations (referred as Fuel 1 and Fuel 2) of the same combustion gas were introduced. PV such as stand-off distance (SoD), powder feed rate, and carrier gas flow were studied through the third WP3 design. Microstructure, microhardness, carbides decarburization, abrasive wear, and corrosion resistance of resulting coatings were evaluated as responses, as well as deposition temperature and relative deposition efficiency. Resulting curvature of Almen strip specimen was also given a particular interest, in order to evaluate residual compressive stress response.

2.3 Characterization Methods

2.3.1 Deposition Temperature. Substrates were positioned on a rotating fixture, equipped with a specially designed wireless thermocouple sensor meter, to acquire on-line deposition temperature on the substrate backside.

2.3.2 Coating Microstructure. SEM micrographs of respective coatings cross sections were analyzed utilizing a

Table 1 Design matrix of experiments

DESIGNS	Reference	Chamber	Injector	Nozzle	Fuel 1, Psi	Fuel 2, Psi	SoD, mm	Feed rate, g/min	Carrier gas, l/min
Design WP1	N1	−1	−1	−1	0	0	0	0	0
	N2	1	−1	−1	0	0	0	0	0
	N3	−1	1	−1	0	0	0	0	0
	N4	1	1	−1	0	0	0	0	0
	N5	−1	−1	1	0	0	0	0	0
	N6	1	−1	1	0	0	0	0	0
	N7	−1	1	1	0	0	0	0	0
	N8	1	1	1	0	0	0	0	0
	N9	1	0	0	0	0	0	0	0*
	N10	1	0	0	0	0	0	0	0*
	N11	1	0	0	0	0	0	0	0*
Design WP2	N1	1	1	0	−1	−1	0	0	0
	N2	1	1	0	1	−1	0	0	0
	N3	1	1	0	−1	1	0	0	0
	N4	1	1	0	1	1	0	0	0
	N5	1	1	0	0	0	0	0	0[a]
	N6	1	1	0	0	0	0	0	0[a]
	N7	1	1	0	0	0	0	0	0[a]
Design WP3	N1	1	1	0	0	0	−1	−1	−1
	N2	1	1	0	0	0	1	−1	−1
	N3	1	1	0	0	0	−1	1	−1
	N4	1	1	0	0	0	1	1	−1
	N5	1	1	0	0	0	−1	−1	1
	N6	1	1	0	0	0	1	−1	1
	N7	1	1	0	0	0	−1	1	1
	N8	1	1	0	0	0	1	1	1
	N9	1	1	0	0	0	0	0	0[a]
	N10	1	1	0	0	0	0	0	0[a]
	N11	1	1	0	0	0	0	0	0[a]

−1 = Low/short; 0 = medium and 1 = high/long
[a]Center points for each respective design

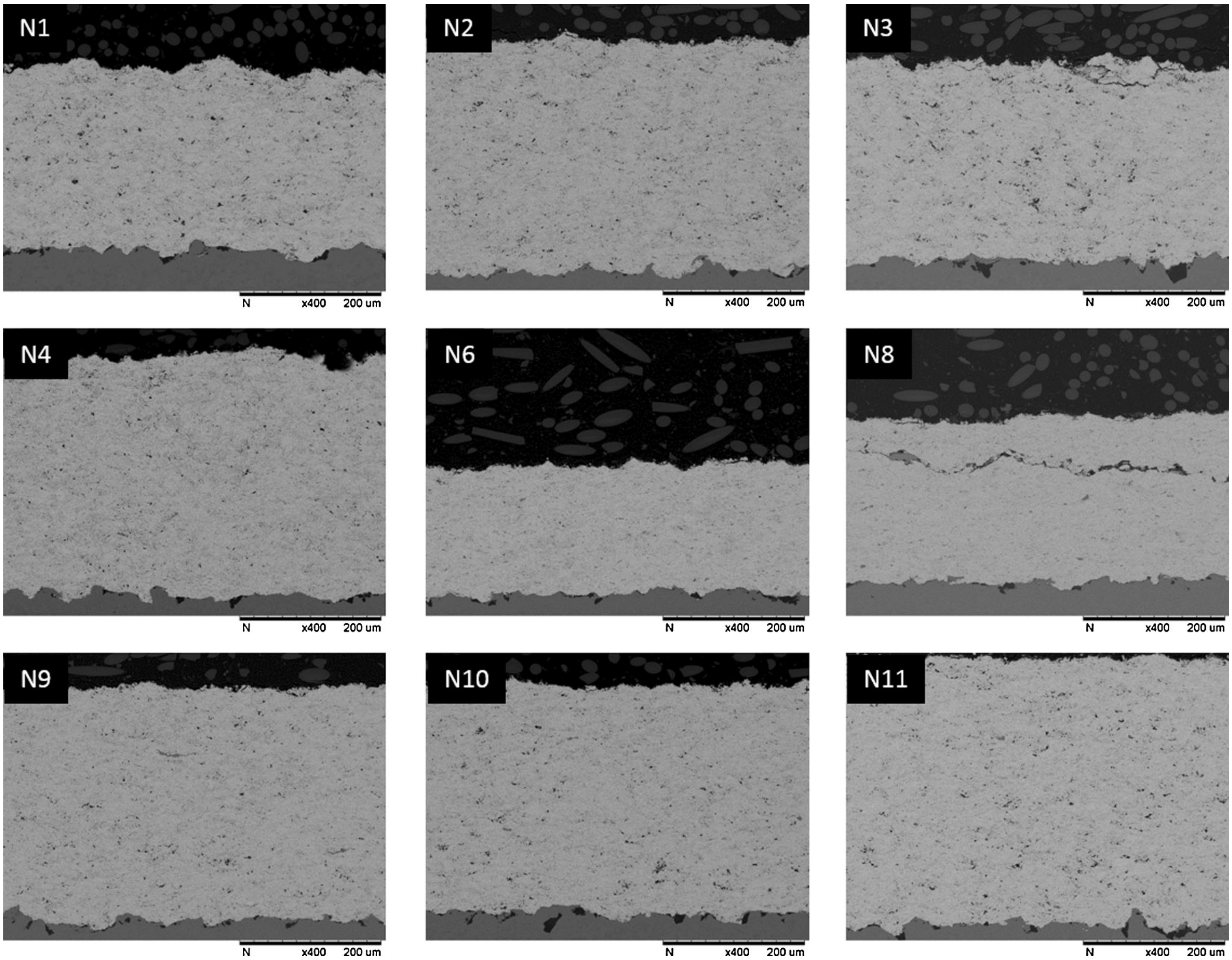

Fig. 1 SEM micrographs for WP1 design

TM3000-Tabletop Microscope (HITACHI). A specially developed image thresholding algorithms utilizing the image analysis Aphelion ® software, were applied on 20 SEM pictures (X7000) per samples, in order to identify volume fraction of porosity and carbide/binder phases, as well as primary carbides size-weighted distributions.

2.3.3 Microhardness Vickers. Micro-Vickers hardness measurements were carried out on the polished cross section of the grit blasted substrates according to ASTM E384-10 with a Vickers indenter at a load of 300 g and dwell time of 15 s, using a Shimadzu Microhardness Tester. HV0.3 was calculated from averaging series of 20 impressions, and respective distributions were analyzed via boxplot representations.

2.3.4 Phase Analysis. X-ray diffraction analysis of powder feedstock and coated systems was carried out using a D500 Siemens diffractometer, with Cr source at 35 kv and 30 mA. Carbides decarburization peaks belonging to W_2C, W, and Co_3W_3C phases were identified and their respective intensities were compared to the WC phase in order to compute the carbide retention index following (Ref 5).

2.3.5 Curvature Measurement. Similar to shot peening evaluations, Almen arc height measurement was carried out utilizing a dedicated Aero gage TSP-3AA for holding paramagnetic specimens on a magnetic Almen gage.

2.3.6 Abrasive Wear Resistance. Dry sand rubber wheel, DSRW, abrasion wear testing was conducted according to the ASTM G65, utilizing standard AFS 50/70 Test Sand from Ottawa Silica Co. (−300 mesh + 212 mesh), under a load of 130.1 N. Three test samples per spray conditions were cut to $70 \times 25\ mm^2$ plates. As-sprayed coated specimens were surface softened during the first 2000 revolutions and weighted wear loss were evaluated for the next 2000 revolutions. Since the density of as-sprayed coatings could not be evaluated in this preliminary work, the respective volume wear loss were not calculated as specified by the ASTM G65, and only weighted wear loss were reported.

2.3.7 Corrosion Resistance. Neutral salt spray test (NSS), formalized as an ASTM B117 following the ISO 9227 standard, was performed to evaluate the relative corrosion resistance of coated materials exposed to a salt spray (pH 6.5-7.2) pre-conditioned to the operating tem-

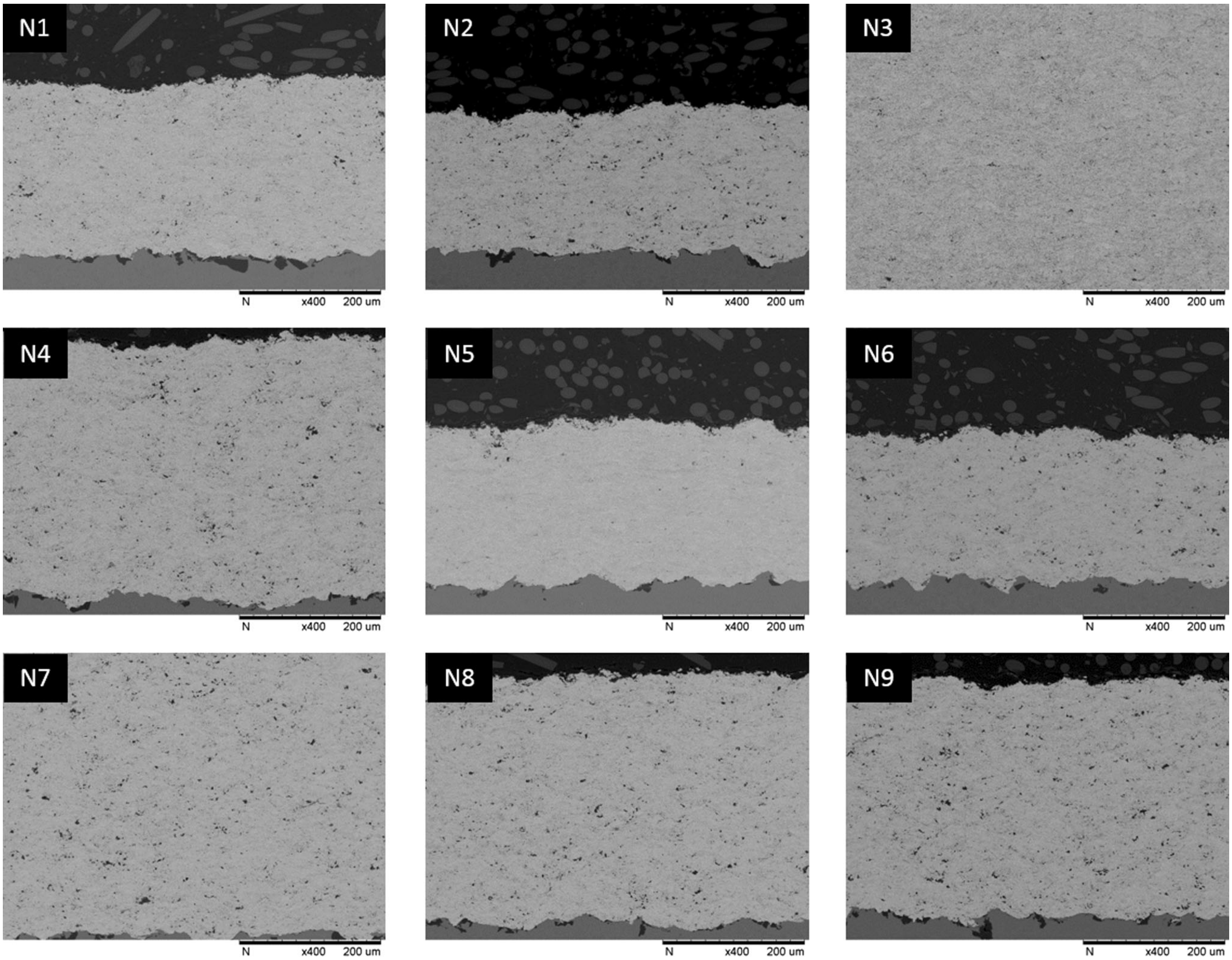

Fig. 2 SEM micrographs for WP3 design

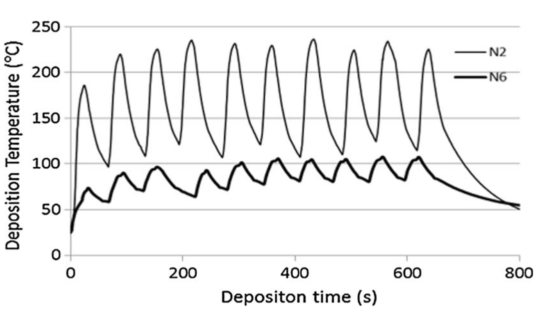

Fig. 3 Deposition Temperature acquisition for N2- and N6-coated systems

perature of 35 ± 2 °C and fogging a 5% salt solution at a condensate collection rate of 1.0 to 2.0 mL/h per 80 m^2. Acetic acid salt spray (ASS) was used for more corrosive environments than the ASTM B117 Standard, according to ISO 16701. A 5% by-mass solution of sodium chloride in 95% of ASTM D1193 Type IV water was used, and the pH was adjusted with the glacial acetic acid between 3.1 and 3.3. This solution was then atomized to create a fog that has a condensate collection rate of 1.0 to 2.0 mL/h per 80 m^2, maintaining the exposure zone to 35 ± 2 °C. Sprayed samples were ground and polished to a Ra of 0.1, edges protected by specially designed tape, and as-polished surface exposed for a maximum period of 216 h (NSS) and 80 h (ASS), respectively.

3. Results and Discussions

Coatings properties were evaluated and discussed in the present section Part I, similar to a conventional parametric study. All the collected have been fed into DoEs in the second section Part II, introducing multi-linear statistical models to establish possible correlation between factors and those responses.

3.1 Part I: Characterization—Responses Evaluation

3.1.1 SEM Microstructure Investigation. Design *WP1:* Two HCs (N5 and N7) failed to obtain a suitable coating

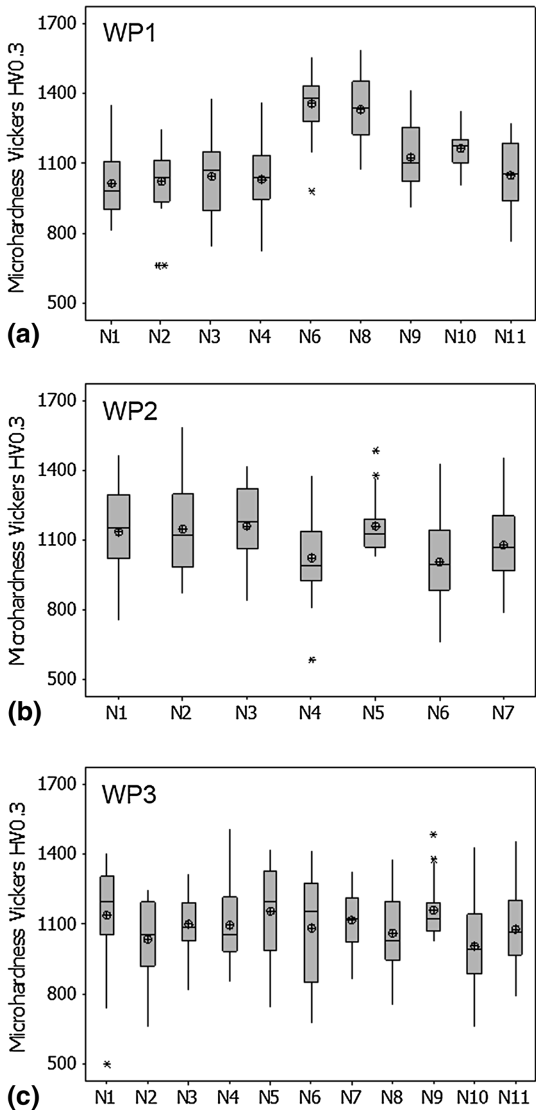

Fig. 4 Boxplot representations of coatings microhardness

deposition while combining short combustion chamber with long nozzle, independent of the length of the powder injector. All other configurations resulted in depositing 250-300 μm of WC-CoCr material, except for the coating N8 and N6, resulting in approximately half the equivalent deposition efficiency. For the latest, combining a short powder injector with a long nozzle did however improve the density of the microstructure, with a porosity level below 0.5%. Increasing the length of the powder injector (sample N8) slightly increased the deposition efficiency; however with a reduction in the particles dwell time, the deposition temperature slightly decreased and the generation of in-plane through-thickness cracks was observed (Fig. 1).

Design *WP2:* Screening the pressure levels of combustion fuels did not lead to obvious differences neither in coating deposition efficiency nor in porosity level. Window of variation of both fuels is extremely limited and constricted to specially designed HCs. The significance of the variation of the porosity level will be investigated in sect. 3.2.

Design *WP3:* This design was screening conventional thermal spray process parameters, such as SoD, powder feed rate, and carrier gas flow. As it could have been expected from the start, higher deposition efficiency was obtained combining shorter SoD and higher feed rate (samples N7 and N3), while the porosity was reduced from 1.9 to 0.8%, respectively, utilizing lower carrier gas flow (Fig. 2). Combining longer SoD and lower feed rate (samples N2 and N6) reduced to half the deposition efficiency for equivalent porosity of 1.6%. The resulting deposition temperature was drastically reduced to 100 °C for sample N6 (Fig. 3), compared to 230 °C for sample N2, while increasing the carrier gas flow which likely acted as an intrinsic cooling system. Effect of increasing the carrier gas flow could not be seen when comparing other couple of samples (N1/N5 and N4/N8), deposited around 230 and 250 °C. Generally speaking, increasing the powder feed rate headed to deposit thicker coatings with equivalent porosity level of 1.6-1.8%, when comparing samples N2 and N4, and respectively samples N6 and N8. Last but not least, the three center points equivalent to sample N9, exhibited intermediate deposition efficiency, porosity level, and deposition temperature, with good repeatability which will strengthen the fit of Multi-linear regression models.

3.1.2 Microhardness Investigation. Boxplot representations of respective distributions of microhardness indentations are useful to highlight outliers' data and compute the average hardness value of the distribution, while its Skewness is described by the position of the median to the quartiles. A narrower distribution stands for higher homogeneity of well-distributed material phases and defects in the coating. At first glance, all coatings from WP1 (Fig. 4a) sprayed with the short nozzle (N1, N2, N3, and N4) exhibited lower average values than the one sprayed with the longer nozzle (N6 and N8). Longer the nozzle, harder the coating with increase of its density, however, to the detriment of the deposition efficiency.

For the second design, the variation of the fuels pressure did not significantly affect the coatings microhardness (Fig. 4b), as previously noticed for porosity levels (Fig. 5). WP3 coatings exhibited dissimilar shape and skewness of respective hardness distributions (Fig. 4c). Narrowest and well-distributed distributions for coatings N3 and N7 were obtained at higher deposition efficiency combining shorter SoD and longer nozzle.

3.1.3 Carbides Retention Index. Respective carbides retention index were computed from XRD diffraction patterns and related to the deposition temperature recorded on substrates backside during the spraying process, as shown in Fig. 3. Carbides decarburization is happening when the powder feedstock material is excessively heated during the manufacturing process, which leads to the formation of unwanted phases, such as W_2C and W. The

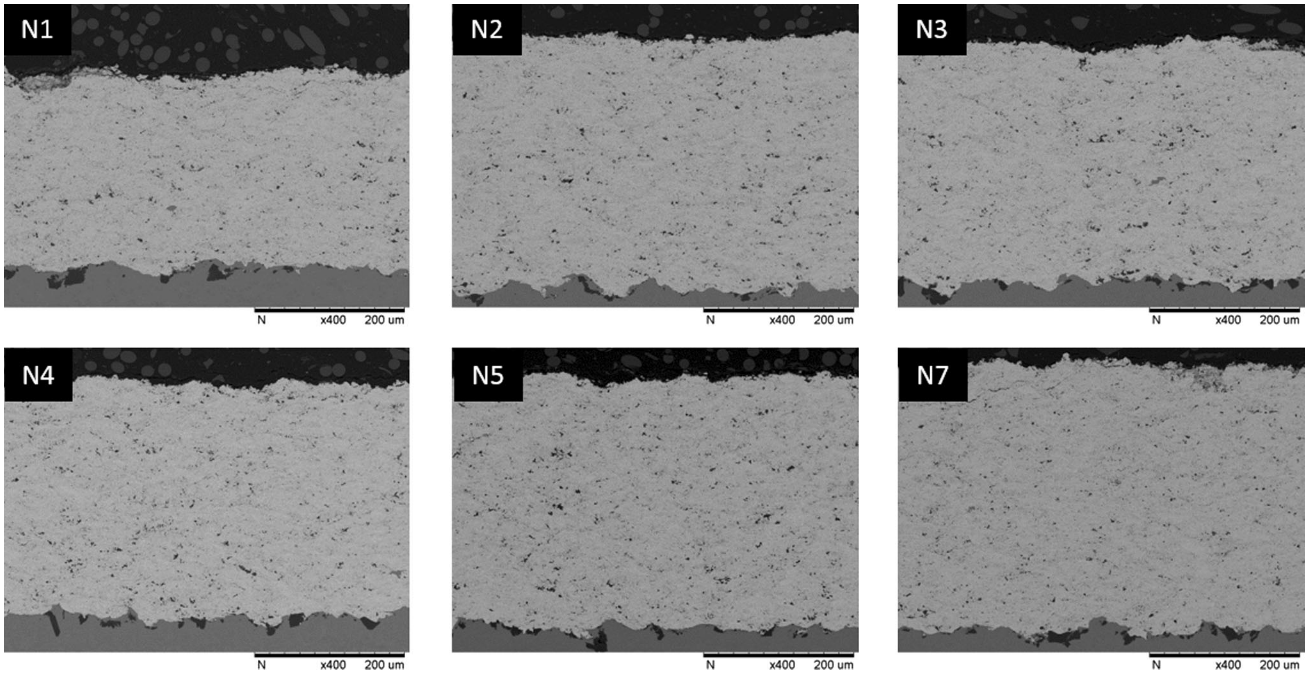

Fig. 5 SEM micrographs for WP2 design

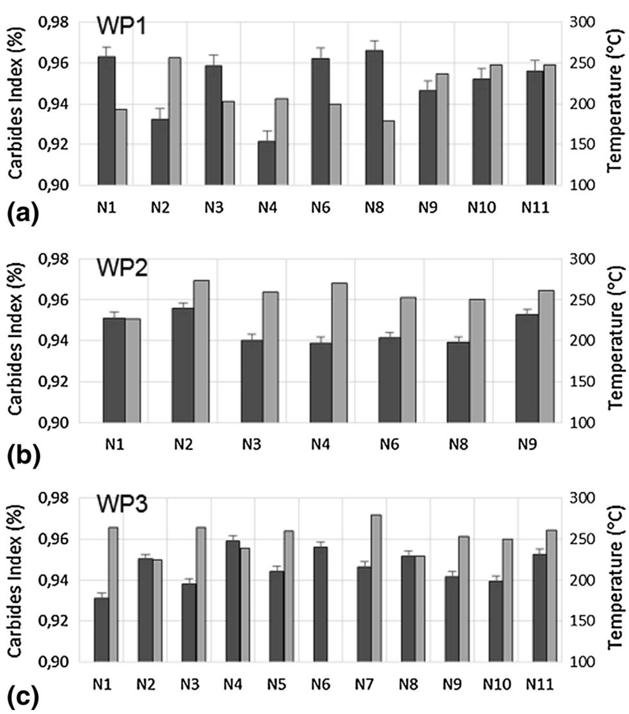

Fig. 6 Carbides retention index—deposition temperature

relative carbides' retention index shows (Fig. 6a) that lower decarburization is obtained with the short combustion chamber (N1-N3), or by combining long chamber and longer nozzle (N6). Utilizing even longer powder injector gave the highest carbide retention index and lowest deposition temperature (Sample N8). Whereas no obvious trends could be perceived for second design WP2 (Fig. 6b), possible relationships will be further analyzed for the third design WP3 (Fig. 6c) regarding the effect of both SoD and powder feed rate on both carbides retention index and deposition temperature.

3.1.4 Wear and Corrosion Resistance. Dry abrasion and corrosion performances of respective coatings have been evaluated for each design (Fig. 7). For the first design WP1, lower wear loss and high NSS corrosion resistance were obtained for the three center points (N9-N10-N11), as well as for coatings N6 and N8 sprayed with larger combustion chamber and longer nozzle (Fig. 7a). The effect of those factors on ASS coating corrosion resistance appeared not to be significant. For the second design WP2, however, relative increase and/or decrease of fuels pressure lead to improve the ASS corrosion resistance of coating compared to the center points (Fig. 7b), whereas NSS and wear resistance did not show significant differences. From the overviewed values of wear and corrosion resistance obtained through the third design WP3 (Fig. 7c), no relationship could be drawn regarding the influence of SoD, feed rate, or carrier gas on coating performances.

3.2 Part II: Design of Experiments: Statistical Evaluation

All previous experimental data were collected and fed into the response matrix for each design, in order to establish relationships between process parameters (factors) and coating properties (responses). In order to describe the impact of factors onto responses, a preliminary multi-linear regression (MLR) fit of the data was plotted for each DoE, where R^2 describes how well the model fits

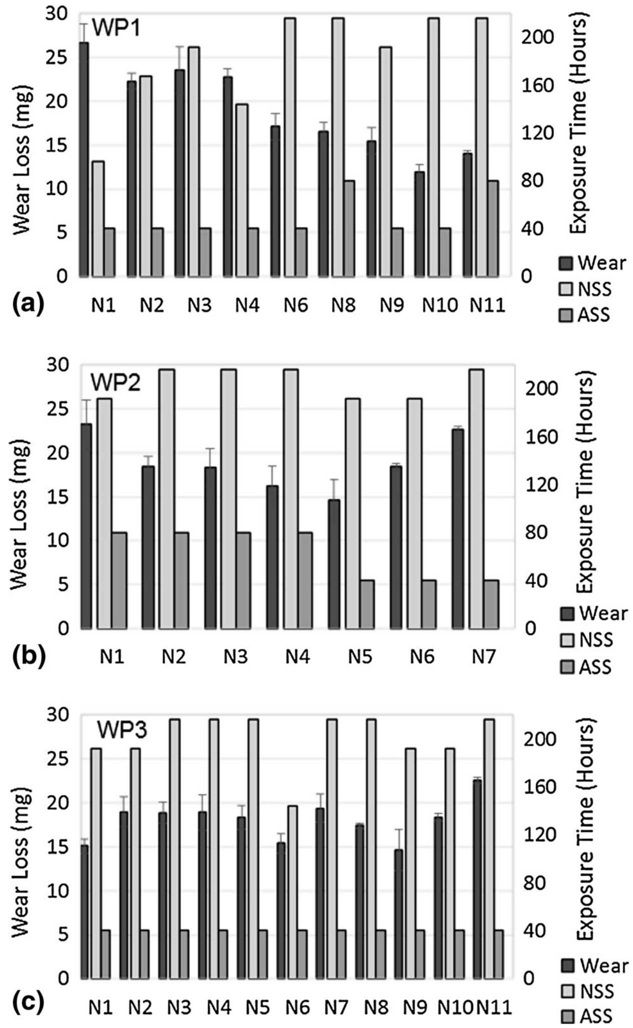

Fig. 7 Abrasion wear and NSS/AASS corrosion results

Table 2 MLR models coefficients for WP1 design

Responses	R^2	Validity	Reproducibility	CI, %
Temperature	0.544	0.057	0.958	95
Thickness	0.617	0.517	0.848	95
Porosity	0.689	0.897	0.356	95
Binder	0.956	0.875	0.894	95
Carbides	0.929	0.770	0.886	95
Ret. Index	0.898	0.764	0.886	95
Microhardness	0.882	0.849	0.806	95
Arc height	0.897	0.360	0.968	95
Wear G65	0.649	0.498	0.871	95
Corr. NSS	0.897	0.671	0.889	95
Corr. AASS	0.563	0.999	0.200	95

the data. The model validity coefficient highlights here the presence of outliers, incorrect or transformation problem for selected response, if its value becomes lower than 0.25. The significance of the weighting coefficient of each factor and their respective interactions on the studied response are also expressed considering the normal distribution of studentized residuals and the replicate index, expressed

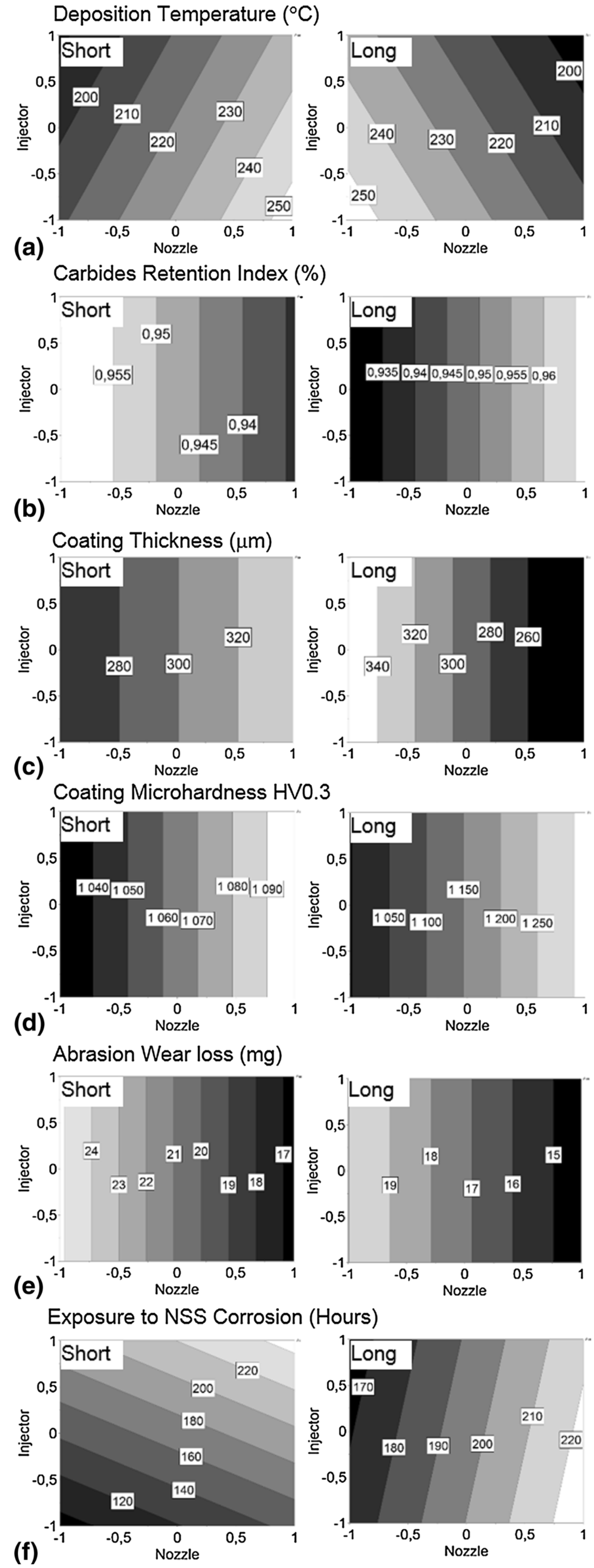

Fig. 8 Contour plots for short and long combustion chambers

Table 3 MLR models coefficients for WP2 design

Responses	R^2	Validity	Reproducibility	CI, %
Temperature	0.950	0.890	0.867	95
Thickness	0.562	0.776	0.144	95
Porosity	0.540	0.889	0.200	95
Binder	0.717	0.700	0.564	95
Carbides	0.711	0.712	0.539	95
Ret. Index	0.618	0.968	0.007	95
Microhardness	0.454	0.878	0.200	95
Arc height	0.513	0.697	0.564	95
Wear G65	0.418	0.984	0.200	95
Corr. NSS	0.292	0.850	0.258	95
Corr. AASS	0.438	0.797	0.167	95

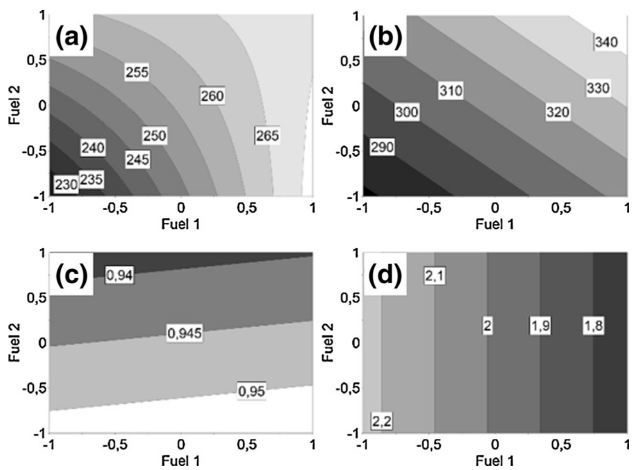

Fig. 9 Contour plots of (a) deposition temperature and (b) coating thickness, (c) retention index and (d) porosity level

Table 4 MLR models coefficients for WP3 design

Responses	R^2	Validity	Reproducibility	CI, %
Temperature	0.534	0.013	0.986	95
Thickness	0.975	0.422	0.995	95
Porosity	0.140	0.681	0.472	95
Binder	0.688	0.954	0.079	95
Carbides	0.444	0.893	0.042	95
Ret. Index	0.673	0.939	0.253	95
Microhardness	0.556	0.935	0.200	95
Arc height	0.814	0.576	0.910	95
Wear G65	0.113	0.985	0.200	95
Corr. NSS	0.512	0.739	0.610	95
Corr. AASS	0.367	0.912	0.200	95

through the Reproducibility variable. The latest variable expresses the variation of the replicates compared to overall variability and warrants a good reproducibility if greater than 0.5. Once the MLR were refitted, each response was represented as a function of the most significant factors' influence, and displayed as contour plots, with a confidence interval (CI) of 95%.

3.2.1 Design of Experiment WP1. Relationships between combustion chamber size, injector and nozzle lengths, and coatings properties have been described by

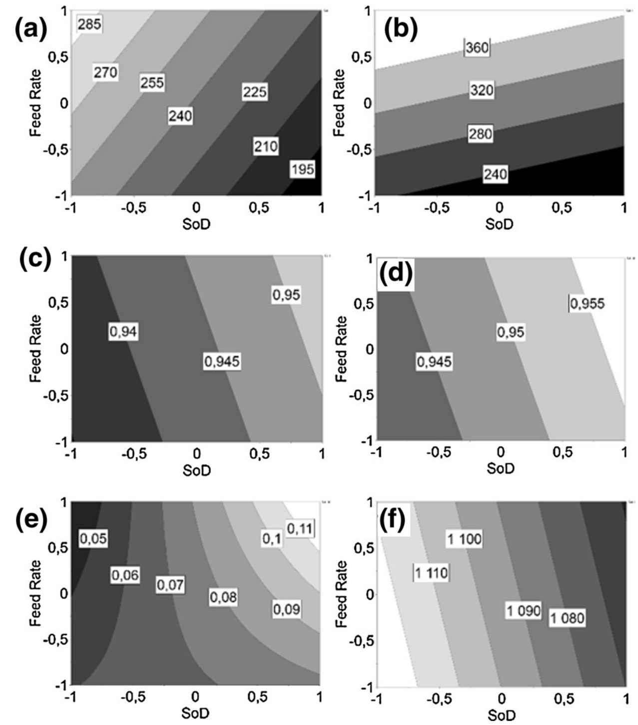

Fig. 10 Contour plots of (a) deposition temperature, (b) coating thickness, Carbides retention index at (c) low and (d) high carrier gas flow, (e) Almen Arc height and (f) coating microhardness Vickers

multi-linear regression (MLR) models for the first design (Table 2). Coefficients of linear regression (R^2) have to be considered very high for the volume fraction and retention index of Carbides, the Almen arc height, coating microhardness, and the NSS corrosion resistance responses. MLR models for abrasion wear resistance, porosity, and coating thickness responses also exhibited relatively good fits. While comparing short combustion chamber with the long , opposite effects on deposition temperature (Fig. 8a), coating thickness (Fig. 8b), and decarburization (Fig. 8c) could be observed. The deposition temperature decreased while increasing the injector length, mostly due to shortening the dwell time. Increasing the nozzle length exhibited opposite effects on the deposition temperature, which (i) increased for short combustion chamber, and (ii) decreased for longer chamber, leading to minimizing the decarburization effect (Fig. 8b). Independent of the injector length, higher deposition efficiency was reached combining either short chamber with long nozzle, or long chamber with short nozzle (Fig. 8c), mostly due to higher deposition temperature. Independent of the injector length, both coating microhardness (Fig. 8d) and abrasion wear resistance (Fig. 8e) significantly augmented with increasing nozzle length; an increase more pronounced for longer combustion chamber compared to short one. NSS coating resistance showed significant improvement with increasing the nozzle length, while combining (i) longer injector with short combustion chamber, and (ii) shorter injector with longer chamber (Fig. 8f). Though the coating porosity response did not show any relationships with the size of the combustion chamber, it is difficult to relate here its effect on the NSS corrosion response. However, the porosity level was significantly reduced from 2.2 to 0.8% with reducing the injector length and increasing the nozzle length, which could explain the previous observation (Fig. 8f).

3.2.2 Design of Experiment WP2. Relationships studied through the second design WP2 (Table 3) demonstrated that the deposition temperature, coating thickness, porosity level, and decarburization responses were significantly influenced by Fuels pressure variation in the studied regime. However, such relationships exhibited a poor reproducibility (<0.5), highlighting the previous comments from sect. 3.1. Higher the Fuel 2 pressure, higher the deposition temperature (Fig. 9a) and consequently, higher the deposition efficiency (Fig. 9b), higher the decarburization (Fig. 9c), whereas no effect on the porosity level could be noticed (Fig. 9d). The porosity level was significantly decreased with increasing the Fuel 1 pressure, with a respectively smaller increase of both the deposition temperature and efficiency than the one noticed while increasing the Fuel 2 pressure.

3.2.3 Design of Experiment WP3. Relationships between SoD, powder feed rate, carrier gas flow, and coatings properties have been described by multi-linear regression (MLR) models for this third design (Table 4). Coefficients of linear regression (R^2) have to be considered very high for the coating thickness, Almen arc height, and the Carbide retention index responses, with a confidence interval of 95%. Contour plots based on derived MLR models for respective responses are shown in Fig. 10. Responses contours are here presented as a function of powder feed rate versus SoD, at a steady and medium carrier gas flow. Variations of the carrier gas flow in the studied regime were not significantly conclusive, except for the carbides retention index response. Shortening the SoD with increasing the powder feed rate leads (i) to increase the deposition temperature (Fig. 10a) and (ii) headed to improve the deposition efficiency up to 40% (Fig. 10b). Higher deposition temperature consequently (i) increases the decarburization process with a decrease of the carbides retention index more pronounced at lower (Fig. 10c) than higher (Fig. 10d) carrier gas flow, and (ii) reduces the residual curvature of the Almen sample (Fig. 10e). The residual curvature obtained at high SoD and high feed rate therefore resulted from the deposition of less-decarburized carbides at lower temperature, which could likely lead to improve the coating microhardness, however, the opposite trend was observed (Fig. 10f). This trend is following the one observed for the porosity level, even if the actual MLR model did not describe well the latest response (Table 4). Higher SoD with higher feed rate leads to an increase in the amount of pores, which participate to the material volume gaged by performing the indentations, and consequently decrease the averaged microhardness values. No significant MLR models could be developed for both abrasion wear and NSS/ASS corrosion responses for this design WP3, which showed low value of regression coefficients (Table 4).

4. Conclusion

WC-CoCr coatings sprayed with the latest HVAF-M3 unit system have been evaluated through several screening designs of experiments. Relationships between several HCs, process parameters, and resulting coating performances were developed, and main results can be summarized as follows:

- Relationships between HCs and coating properties were derived: longer the injector, lower the deposition temperature. While increasing the length of the nozzle, the deposition temperature (i) increases with short combustion chamber, and (ii) decreases when utilizing longer chamber, leading for both cases to improve the coating microhardness and abrasion wear resistance. Colder conditions headed to improve deposition efficiency and minimize decarburization phenomena. NSS corrosion resistance of the coating increased with combining (i) longer injector with short combustion chamber, and (ii) shorter injector with longer chamber.
- Relationships between fuels pressure and coating properties were as well developed: increase of both the Fuel 1 and Fuel 2 pressures headed to increase the deposition temperature, and improve the ASS corrosion resistance of the coatings. The lack of fit of developed MLR models for the other responses demonstrates that in the studied regime of variation, Fuel 1 and Fuel 2 do not significantly influence the coating porosity level,its decarburization, or its microhardness neither its abrasion wear resistance.
-]Last but not least, relationships between conventional process parameters and coating properties were established. Higher the powder feed rate and shorter the SoD, higher the deposition temperature and higher the deposition efficiency. Consequently, higher carbides retention index was obtained at higher SoD, with a small but significant increase at higher feed rate and higher carrier gas flow. Shortening the SoD increases both particles impingement at high velocities (and therefore the resulting microhardness) and the deposition temperature, which consequently (i) increases decarburization phenomena, but (ii) as well accommodates the compression stresses induced by shortening the SoD, emphasized by the decreasing arc height of the Almen strip samples.

Acknowledgments

The authors would like to express their gratitude to Sulzer Metco for providing the powder feedstock material and carrying out the ASTM G65 abrasion wear test. Stefan Björklund is gratefully acknowledged for his help in processing, engineering, and developing our HVAF ther-

Peer Reviewed

Peer Reviewed

mal spray resources at University West and Production Technology Centre in Trollhättan, Sweden.

References

1. M. Bielewski, *Replacing Cadmium and Chromium, Research and Technology Organisation and NATO, RTO-AG-AVT-140* (2011), Chp. 23, p 1-22
2. L. Lusvarghi, G. Bolelli, T. Börner, C. Lyphout, N. Markocsan, P. Nylén, H. Koivuluoto, P. Sassatelli, P. Vuoristo, S. Zimmermann, and L.M. Berger, *Tribology of HVOF- and HVAF-sprayed WC-CoCr Hardmetal Coatings: a comparative assessment, World Tribology Conference*, Torino, Italy, 2013
3. K.O. Legg, Overview of Chromium and Cadmium Alternative Technologies, *Proceedings of the International Conference on Surface Modification Technologies*, 15th, ASM International, Materials Park, OH, 2002, p 235-244
4. G. Bolelli, L.M. Berger, M. Bonetti, and L. Lusvarghi, Comparison Study of the Dry Sliding Wear Behaviour of HVOF-Sprayed WC-(W, Cr)2C-Ni and WC-CoCr Hardmetal Coatings, *Wear*, 2014, **309**, p 96-111
5. C. Bartuli, T. Valente, F. Cipri, E. Bemporad, and M. Tului, Parametric Study of an HVOF Process for the Deposition of Nanostructured WC-Co Coatings, *J. Thermal Spray Technol.*, 2005, **14**, p 187-195
6. I. Hulka, V.A. Serban, I. Secosan, P. Vuoristo, and K. Niemi, Wear Properties of CrC-37WC-18M Coatings Deposited by HVOF and HVAF Spraying Processes, *Surf. Coat. Technol.*, 2012, **210**, p 15-20
7. Lyphout C., S. Björklund, and P. Boccaccio, *Optimization of Gritblasting Conditions by Supersonic Air Spraying, ITSC*, Barcelona, Spain, 2014
8. C. Lyphout, J. Kitamura, K. Sato, and S. Dizdar, *Tungsten Carbide Deposition Processes for Hard Chrome Alternative: Preliminary Study of HVAF vs. HVOF Thermal Spray Processes*, ITSC, Busan, South Korea, 2013
9. C. Lyphout and K. Sato, *Optimization of W-based HVAF-Sprayed Coatings for Alternative to hard Chromium: Role of Carbides Grain Size and Mean Free Path on Coating Wear and Corrosion Properties*, ITSC, Barcelona, Spain, 2014